MOLECULAR AND CELLULAR BIOLOGY, Dec. 2006, p. 9003–9015 Vol. 26, No. 23
0270-7306/06/$08.00+0 doi:10.1128/MCB.01811-05

Normal Establishment of Epithelial Tight Junctions in Mice and Cultured Cells Lacking Expression of ZO-3, a Tight-Junction MAGUK Protein▽‡§

Makoto Adachi,[1]†* Akihito Inoko,[1]† Masaki Hata,[2] Kyoko Furuse,[2] Kazuaki Umeda,[1] Masahiko Itoh,[1] and Shoichiro Tsukita[1]

Department of Cell Biology, Faculty of Medicine, Kyoto University, Sakyo-ku, Kyoto 606-8501, Japan,[1] and KAN Research Institute, Inc., Kyoto Research Park, Chudoji, Shimogyo-ku, Kyoto 600-8815, Japan[2]

Received 15 September 2005/Returned for modification 19 November 2005/Accepted 1 September 2006

ZO-1, ZO-2, and ZO-3 are closely related MAGUK family proteins that localize at the cytoplasmic surface of tight junctions (TJs). ZO-1 and ZO-2 are expressed in both epithelia and endothelia, whereas ZO-3 is exclusively expressed in epithelia. In spite of intensive studies of these TJ MAGUKs, our knowledge of their functions in vivo, especially those of ZO-3, is still fragmentary. Here, we have generated mice, as well as F9 teratocarcinoma cell lines, that do not express ZO-3 by homologous recombination. Unexpectedly, *ZO-3*$^{-/-}$ mice were viable and fertile, and rigorous phenotypic analyses identified no significant abnormalities. Moreover, *ZO-3*-deficient F9 teratocarcinoma cells differentiated normally into visceral endoderm epithelium-like cells in the presence of retinoic acid. These cells had a normal epithelial appearance, and the molecular architecture of their TJs did not appear to be affected, except that TJ localization of ZO-2 was upregulated. Suppression of ZO-2 expression by RNA interference in *ZO-3*$^{-/-}$ cells, however, did not affect the architecture of TJs. Furthermore, the speed with which TJs formed after a Ca^{2+} switch was indistinguishable between wild-type and *ZO-3*$^{-/-}$ cells. These findings indicate that ZO-3 is dispensable in vivo in terms of individual viability, epithelial differentiation, and the establishment of TJs, at least in the laboratory environment.

Epithelial cells are connected side-by-side by junctional complexes consisting of tight junctions (TJs), adherens junctions (AJs), and desmosomes from the apical side (10). Among these intercellular junctions, TJs are thought to be at least bifunctional: TJs create a primary barrier to the diffusion of solutes through the paracellular pathways (barrier function) and maintain the asymmetry of apical versus basolateral plasma membrane domains by restricting the movement of integral membrane proteins and lipids within plasma membranes (fence function) (1, 4, 43, 50). Thus, TJs are prerequisite for epithelial cells to exert their barrier function and are indispensable for multicellular organisms to survive.

On freeze-fracture electron microscopy, TJs are identified as a series of continuous, anastomosing intramembranous particle strands that are called TJ strands or fibrils (44). A growing number of molecules have now been identified as structural components of TJ strands. Among these, occludin (12), claudins (11), JAM/JAM-related immunoglobulin G-superfamily proteins (8, 32), and tricellulin (19) are classes of integral membrane proteins of TJ strands. Claudins, which bear four transmembrane domains with both NH_2 and COOH termini located in the cytoplasm, comprise a gene family that consists of 24 members and directly contribute to the structure and functions of TJ strands (11, 34, 49, 50). In contrast, information on occludin, which also bears four membrane-spanning domains, and JAM, a single-pass transmembrane protein, is still fragmentary. Tricellulin, which has four transmembrane domains, is unique in that it is mostly concentrated at tricellular contacts of TJ strands.

Several peripheral membrane proteins underlying the cytoplasmic surface of TJs have also been identified and are believed to be involved in the formation of TJs or in the intracellular signaling originating from TJs. In general, these proteins have domains responsible for protein-protein interactions, such as a PDZ (for PSD95/Dlg/ZO-1) domain, and are thought to make up macromolecular complexes connecting to TJ integral membrane proteins through these domains (33, 39, 50). Among them, three closely related PDZ domain-containing proteins, ZO-1, -2, and -3, have attracted increasing interest. They contain three PDZ domains (PDZ1, -2, and -3), one Src homology 3 (SH3) domain, and one guanylate kinase-like (GUK) domain from their NH_2 termini and so are called MAGUKs (for membrane-associated guanylate kinase proteins) (Fig. 1A) (3, 14, 15, 17, 45). All of them bind to the cytoplasmic tail of claudins at their PDZ1 domain and also to actin filaments in their COOH-terminal region (13, 17, 21, 22, 53). Molecules involved in the establishment of epithelial polarity are also concentrated at TJs: Par3/Par6/atypical protein kinase C (aPKC) and Crb3/Pals1/Patj complexes localize at TJs (24, 25, 26, 28, 29, 31, 41). Furthermore, several other proteins such as cingulin (7), JACOP (37), JEAP (36), MUPP1 (16), ZONAB (5), and GEF-H1/Lfc (6) are also reported as peripheral membrane proteins of TJs, though their physiological functions have not yet been substantially defined.

* Corresponding author. Mailing address: Department of Cell Biology, Faculty of Medicine, Kyoto University, Sakyo-ku, Kyoto 606-8501, Japan. Phone: 81-75-753-4375. Fax: 81-75-753-4660. E-mail: ada@mfour.med.kyoto-u.ac.jp.

† M.A. and A.I. contributed equally to this study.

‡ Supplemental material for this article may be found at http://mcb.asm.org/.

§ Dedicated to the memory of coauthor Shoichiro Tsukita, now deceased.

▽ Published ahead of print on 25 September 2006.

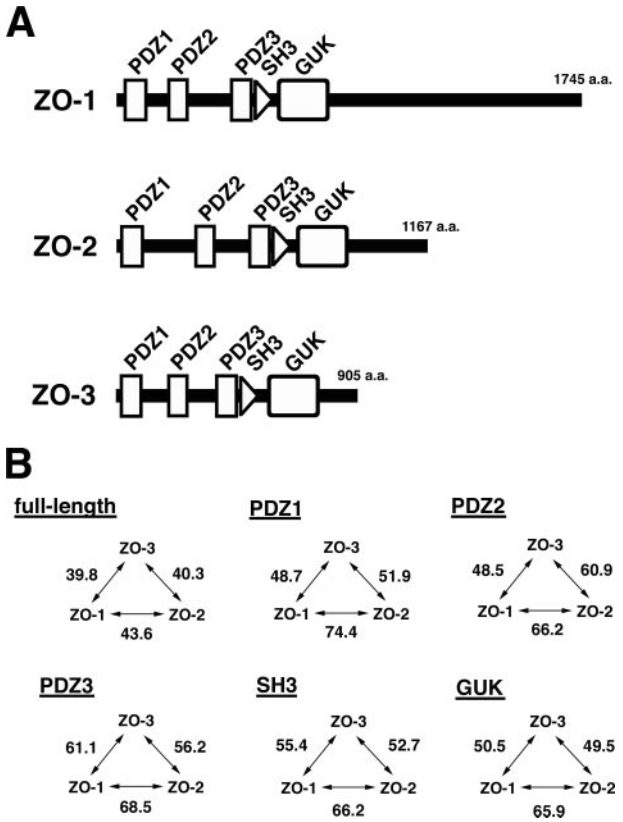

FIG. 1. Schematic representation of ZO-1, ZO-2, and ZO-3. (A) Domain organization of three TJ MAGUKs. They have three PDZ domains, one SH3 domain, and one GUK domain in this order from their NH_2 termini in common. (B) Amino acid sequence identities between the three MAGUKs. The values shown are percent identities between the full-length and the respective domains of these proteins. Although these proteins have significant structural similarity, the overall similarity between ZO-3 and ZO-1 and between ZO-3 and ZO-2 was slightly weaker than the similarity between ZO-1 and ZO-2. Identity values were calculated by using Genetyx Mac software.

Among the three TJ MAGUKs, only ZO-3 is specifically expressed in epithelia (20). ZO-1 and ZO-2 are, in addition to TJs of the epithelia or endothelia, concentrated at spot-like AJs of fibroblasts, intercalated discs of cardiac muscle cells, and the outer limiting membranes of the retina, but ZO-3 was undetectable in these cells. Northern blot analysis shows that ZO-3 is expressed abundantly in the lung, the liver, and the kidney and, according to the public EST database, ZO-3 appears to be expressed in large amounts in the colon, the stomach, and other epithelial organs (20). Although the three MAGUKs have considerable structural homology, a calculation of amino acid sequence identity has revealed that the structural similarity between ZO-3 and ZO-1 or between ZO-3 and ZO-2 was lower than the similarity between ZO-1 and ZO-2 (Fig. 1B). Thus, ZO-3 appears to have its own specific molecular properties. However, the functional characteristics of ZO-3 have been examined less than those of ZO-1 and ZO-2. Overexpression of the NH_2-terminal half of ZO-3 containing the PDZ1, -2, and -3 domains in MDCK cells reportedly induces remarkable changes in the organization of actin cytoskeletons and delays the assembly of TJs and AJs during epithelial polarization (54, 55). Furthermore, ZO-3 was reported to directly bind to the PDZ6 domain of Patj at its COOH terminus. When this PDZ domain was deleted from Patj, the resultant truncated Patj was not recruited to TJs, suggesting that ZO-3 is involved in the epithelial polarization by recruiting Patj and its binding partners to TJs (40).

Here we generated mice, as well as mouse teratocarcinoma F9 cells, that lack the expression of ZO-3, by homologous recombination. *ZO-3*-deficient mice were viable and fertile. Intensive analyses revealed that there were no significant histological abnormalities in any of the organs examined. Moreover, when *ZO-3*-deficient F9 cells were suspension cultured in the presence of retinoic acid (18), they differentiated normally to form visceral endoderms. Electron microscopy identified normal TJs, and immunofluorescence microscopy revealed a normal molecular architecture of TJs. Furthermore, a Ca^{2+} switch experiment has shown that ZO-3 is indispensable for the assembly of TJs. Therefore, we concluded that ZO-3 is dispensable not only at the cellular level but also at the whole body level in mice.

MATERIALS AND METHODS

Targeting strategy. A λ phage 129/Sv mouse genomic library was screened by using a mouse ZO-3 cDNA fragment as a probe, and the overall structure of the mouse ZO-3 genomic locus was determined as shown in Fig. 2A. Two types of targeting vectors were constructed. Targeting vector I was designed to delete all exons except exon 1 and was used for targeting the first allele of the *ZO-3* gene in embryonic stem (ES) cells and F9 cells (see Fig. 2A and 5A). Targeting vector II was designed to insert the targeting vector cassette into exon 3 and was used for targeting the second allele of *ZO-3* in F9 cells (see Fig. 5A). To construct targeting vector I, a 15.5-kb XhoI-NotI fragment (5′ arm) and a 0.94-kb HindIII-ApaI fragment (3′ arm), were, respectively, ligated to the 5′ and 3′ sides of the targeting vector cassette, which contains a promoterless lacZ cassette and a PGK-Neo (neomycin resistance gene) cassette (opposite to the orientation of the *ZO-3* gene and flanked by loxP sequences). The diphtheria toxin A expression cassette (MC1pDT-A) was placed outside the 3′ arm for negative selection. To construct targeting vector II, the 15.5-kb XhoI-NotI fragment (5′ arm) and a 1.1-kb SacII-ApaI fragment (3′ arm) were ligated to the targeting cassette, which contains IRES, lacZ, and PGK-Neo (opposite orientation, flanked by loxP sequences) cassettes. The DT-A cassette was placed outside the 3′ arm.

To generate mice lacking the expression of ZO-3, J1 ES cells were electroporated with targeting vector I (linearized by XhoI digestion) and selected for ~9 days in the presence of G418. The G418-resistant colonies were removed and screened by Southern blotting with the 3′ external probe (3′probe-1) (see Fig. 2A). Correctly targeted ES clones were identified by an additional 5.4-kb band together with the 9.8-kb band of the wild-type allele when digested with EcoRI. The targeted ES cells obtained were injected into C57BL/6 blastocysts, which were in turn transferred into BALB/c foster mothers to obtain chimeric mice. Male chimeras were mated with C57BL/6 females, and agouti offspring were genotyped to confirm the germ line transmission of the targeted allele. The littermates were genotyped by Southern blotting. Heterozygous mice were then interbred to produce homozygous mice.

To generate *ZO-3*-deficient F9 cells, parental F9 cells were electroporated with targeting vector I (linearized with XhoI) and selected for 7 days in the presence of G418 (Fig. 5A). The G418-resistant colonies were removed and screened by PCR using primers that surround the 3′ side of the insertion site of the targeting cassette (ZO3ATV63′-2; 5′-TCCCAGGTTTGCATCCAGAAG C-3′ and TV6-PGK3; 5′-GTGGATGTGGAATGTGTGCGAG-3′) to produce a 1.0-kb band only from the targeted allele. For confirmation, the PCR-positive clones were further examined by Southern blotting with 3′probe-1 as described above. The single-targeted cells obtained were transfected with pCRE-PAC (47) and cultured for 2 days to obtain the "Cre allele" (see Fig. 5A). Cells were selected for 2 days in the presence of puromycin (1 μg/ml). Then, puromycin was removed from the medium, and the cells were further cultured for ~7 days. Colonies grown were removed and tested as to whether they die in the presence of G418, i.e., whether the PGK-Neo cassette was successfully removed from the targeting cassette by the Cre treatment, and whether they die in the presence of puromycin, i.e., whether the pCRE-PAC vector is not stably integrated into the

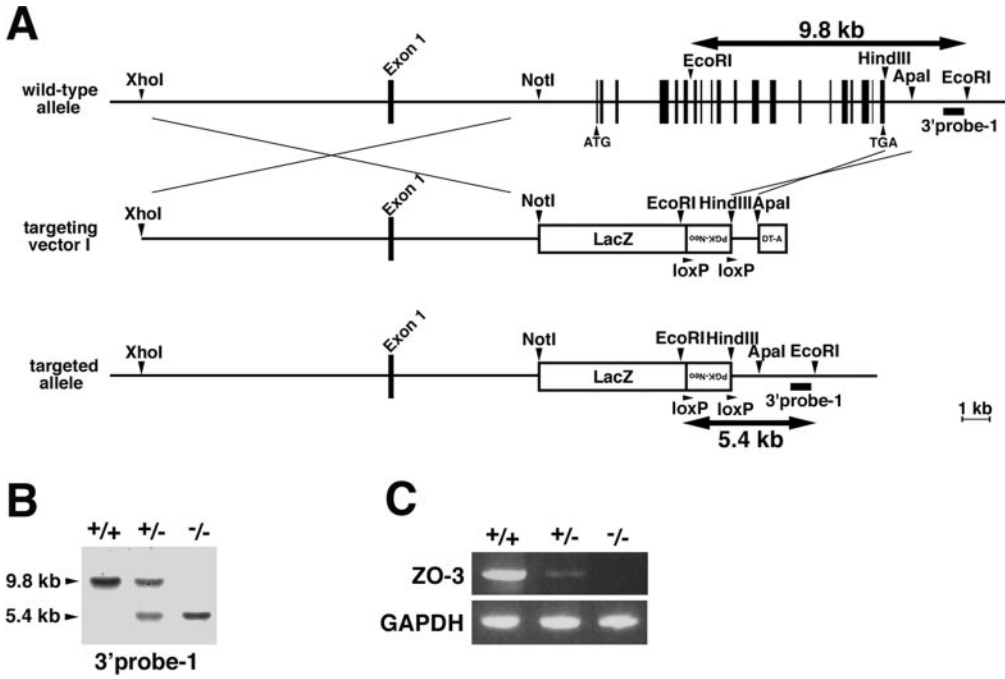

FIG. 2. Generation of *ZO-3*$^{-/-}$ mice. (A) Restriction maps of the wild-type allele, the targeting vector (targeting vector I), and the targeted allele of the mouse *ZO-3* gene. The *ZO-3* gene is composed of 21 exons, and the first ATG and the stop TGA codons are located in the putative exons 2 and 21, respectively. Targeting vector I contains the LacZ/PGK-Neo cassette in its middle portion to delete all exons that encompass the ORF of ZO-3, i.e., exon 2 to exon 21, in the targeted allele. The position of the 3′ probe for Southern blotting (3′probe-1) is indicated as bars. (B) Genotype analyses by Southern blotting of EcoRI-digested genomic DNA from wild-type (+/+), heterozygous (+/−), and homozygous (−/−) mice with respect to the mutant *ZO-3* gene allele. Southern blotting with 3′probe-1 yielded a 9.8-kb band from the wild-type allele and a 5.4-kb band from the targeted allele. (C) Loss of ZO-3 mRNA in the kidney of *ZO-3*$^{-/-}$ mice examined by RT-PCR. A set of primers that correspond to the sequences within exon 18 and exon 21 was used. A single product with a predicted length was obtained from wild-type (+/+) and heterozygous (+/−) mice but not from homozygous (−/−) mice. As a control, the glyceraldehyde-3-phosphate dehydrogenase (GAPDH) gene was equally amplified in all samples.

genome. The clones that were sensitive to both drugs were further examined by Southern blotting with 3′probe-1 to confirm the lack of a PGK-Neo cassette (see Fig. 5). These clones were identified by a 3.4-kb band instead of a 5.4-kb band. These singly targeted F9 cells were then electroporated with targeting vector II (linearized with XhoI) and selected as described above. Screening was performed by PCR using primers that surround the 3′ side of the insertion site of the targeting cassette (ZO3TV12-3′-3; 5′-TAGAATCCCCTAGTGAGGGTCC-3′ and TV6-PGK3) to produce a 1.0-kb band only from the targeted allele. Finally, PCR-positive clones were examined by Southern blotting with 3′probe-2 (see Fig. 5). Correctly targeted alleles were identified by a 3.9-kb band instead of a 7.1-kb band when digested with PstI.

To check that targeting vectors were not randomly integrated into the genome, Southern blotting was performed with the internal Neo-probe, and a lack of random integration was corroborated in both ES and F9 cells.

Reverse transcription-PCR (RT-PCR). Total RNA isolation and first-strand cDNA synthesis were conducted as described previously (34). For subsequent PCR, the following sets of primers were used: 5′-GGAAGAGCTGACCATCT GGGAACAACACAC-3′ (positions 3 to 32 of the ZO-3 open reading frame [ORF], encoded in exon 2 of *ZO-3*, upstream) and 5′-GGACTACTGCGCCCT ACAGATCTGCAGCC-3′ (complementary sequence of the 5′ terminus of the targeting cassette of targeting vector II, downstream), 5′-CGGGGACCACATC GTCATGGTGAATGGTG-3′ (positions 162 to 190 of ZO-3 ORF, encoded in exon 4, upstream) and 5′-CACCAGCACGGACTTTAGTGGCCTCATTAG-3′ (complementary sequence of positions 541 to 570 of the ZO-3 ORF, encoded in exon 5, downstream), and 5′-CAACAGCAGGCGCGACCGATCTGGACCGC G-3′ (positions 2263 to 2292 of the ZO-3 ORF, encoded in exon 18, upstream) and 5′-CAGGTCGGTGGCTGGGCCCCAGTCATAGCC-3′ (complementary sequence of positions 2686 to 2715 of the ZO-3 ORF, encoded in exon 21, downstream). GAPDH was amplified by using 5′-GAGCTGAACGGGAAGCT CACTGGCATGGCC-3′ (upstream) and 5′-CTCCTTGGAGGCCATGTAGG CCATGAGGTC-3′ (downstream).

Cells and antibodies. Mouse teratocarcinoma F9 cells were grown in Dulbecco modified Eagle medium supplemented with 10% fetal calf serum on gelatin-coated culture dishes. Visceral endodermal differentiation was performed essentially as described previously (27, 30). Briefly, for embryoid body formation, after cells in suspension (1.5×10^3 cells/aggregate) were cultured in the presence of 5×10^{-8} M retinoic acid by hanging-drop culture for 3 days, cell aggregates were cultured on noncoated culture dishes in medium containing the same concentration of retinoic acid for ca. 4 to 6 days. For differentiation under monolayer culture conditions, cells were plated at a density of 6×10^3 cells/cm^3. On the next day, 10^{-6} M of retinoic acid was added to the medium and cultured in the presence of retinoic acid for an additional 7 days.

Mouse anti-ZO-1 monoclonal antibody (MAb; T8-754) (23), rat antioccludin MAb (MOC37) (42), rat anti-ZO-3 MAb (20), and mouse anticingulin MAb (37) were raised and characterized previously. Rabbit anti-Par6β polyclonal antibody (PAb; BC32AP), rabbit anti-Patj PAb, and rat anti-E-cadherin MAb (ECCD2) were provided by S. Ohno (Yokohama city University, Yokohama, Japan), A. Le Bivic (University of Marseille, Marseille, France), and M. Takeichi (Center for Developmental Biology, Kobe, Japan), respectively. Rabbit anti-ZO-2 PAb (H-110; Santa Cruz Biotechnologies, Inc.), mouse anti-ZO-2 MAb (BD Transduction Laboratories, Inc.), and rabbit anti-claudin-3 PAb, mouse anti-claudin-4 MAb, rabbit anti-ZO-1 PAb, and rabbit anti-ZO-3 PAb (Zymed Laboratories, Inc.) were obtained commercially.

RNA interference. The shRNAi vector for mouse ZO-2, in which the sequence from positions 946 to 977 of mouse ZO-2 mRNA was subcloned into the downstream of the U6 promoter, was designed and constructed as described previously (51). This vector was stably transfected into wild-type and *ZO-3*$^{-/-}$ F9 cells.

Immunofluorescence microscopy. Mouse tissues were frozen by using liquid nitrogen. Frozen sections ~5 μm thick were cut on a cryostat, mounted on glass slides, air dried, and fixed in 95% ethanol at 4°C for 30 min, followed by treatment with 100% acetone at room temperature for 1 min. The sections were

TABLE 1. Genotypic analysis of offspring from heterozygous/heterozygous breeding pairs[a]

Genotype	No. (%) of mice
+/+	11 (23.9)
+/−	21 (45.7)
−/−	14 (30.4)

[a] Offspring from seven breeding pairs were analyzed.

washed with phosphate-buffered saline (PBS) three times and then blocked with 3% bovine serum albumin-PBS for 30 min and incubated with primary antibodies. After being washed with PBS another three times, samples were incubated with secondary antibodies for 30 min.

F9 cell aggregates were fixed either in 3% formalin for 30 min at room temperature, in 10% trichloroacetic acid for 30 min at 4°C, or in methanol for 10 min at −20°C. When fixed with formalin or trichloroacetic acid, aggregates were treated with 0.2% Triton X-100–PBS for 5 min. They were then processed for immunofluorescence microscopy as described above. The aggregates were examined with an Olympus BX51 photomicroscope (Olympus) or a Zeiss LSM510 confocal laser-scanning microscope (Carl Zeiss).

Histological analyses. Mouse tissues were fixed with 10% formalin-PBS for 3 days at 4°C. Samples were then dehydrated through a graded series of ethanol, and embedded in paraffin wax. Sections ~5 μm thick were cut on a microtome and stained with hematoxylin-eosin and/or periodic acid-Schiff.

RESULTS

Generation of *ZO-3*-deficient mice. To explore the function of ZO-3 in vivo, we produced mice lacking its expression. By using the ZO-3 cDNA fragment as a probe, we isolated the mouse *ZO-3* gene from a λ phage 129/Sv mouse genomic library. Nucleotide sequencing and restriction enzyme mapping revealed that the *ZO-3* gene consists of 21 exons: the putative exon 2 contains the first ATG codon, and the stop TGA codon is located within exon 21 (Fig. 2A). We then constructed targeting vector I, designed to replace all exons except for exon 1 with the LacZ/PGK-Neo (neomycin resistance gene) cassette. In the targeted allele, the ORF of ZO-3 is expected to be completely removed. One line of mice was generated from an ES cell clone in which the *ZO-3* gene was disrupted by homologous recombination. Southern blotting revealed the *ZO-3* gene to be disrupted in heterozygous (*ZO-3*$^{+/-}$) and homozygous (*ZO-3*$^{-/-}$) mice (Fig. 2B). RT-PCR analysis confirmed a lack of ZO-3 expression in *ZO-3*$^{-/-}$ mice (Fig. 2C). There was no obvious phenotype in *ZO-3*$^{+/-}$ mice, and when these mice were interbred, *ZO-3*$^{+/+}$, *ZO-3*$^{+/-}$, and *ZO-3*$^{-/-}$ mice were born in the expected Mendelian ratio (Table 1). *ZO-3*$^{-/-}$ mice did not show any abnormalities. They had a normal body weights, well-groomed coats, and normal body postures and showed normal behavior. The blood and urine were also examined, but no abnormalities were detected. When *ZO-3*$^{-/-}$ females were mated with *ZO-3*$^{-/-}$ males, they produced litters normally, indicating that *ZO-3*$^{-/-}$ mice are fertile.

TJs in *ZO-3*$^{-/-}$ mice. We first examined the structure of TJs in the small intestine as representative of the epithelial tissues. Ultrathin-section electron microscopy revealed that the *ZO-3*$^{-/-}$ intestinal epithelial cells were well polarized with characteristic apical membranes bearing numerous and regularly arranged microvilli. They were indistinguishable from the *ZO-3*$^{+/+}$ intestinal epithelial cells (Fig. 3Aa and a′). Furthermore, close inspection failed to detect any difference in the morphology of the junctional complexes, including TJs between *ZO-3*$^{+/+}$ and *ZO-3*$^{-/-}$ cells (Fig. 3Ab and b′). Immunofluorescence microscopy revealed that, in *ZO-3*$^{-/-}$ intestinal epithelial cells, occludin (Fig. 3B) and ZO-1 (data not shown) were normally concentrated in the most apical part of lateral membranes showing a typical honeycomb pattern, although ZO-3 became completely undetectable in TJs. Similarly, also in *ZO-3*$^{-/-}$ renal tubules, ZO-1 (Fig. 3C) and occludin (data not shown) were exclusively concentrated at TJs lacking ZO-3. Finally, immunoblotting of lysates of kidney of *ZO-3*$^{+/+}$ and *ZO-3*$^{-/-}$ mice revealed that the expression levels of several junction-associated proteins were mostly indistinguishable between *ZO-3*$^{+/+}$ and *ZO-3*$^{-/-}$ mice (Fig. 3D). Therefore, we conclude that *ZO-3*-deficiency did not affect the morphology or the molecular assembly of TJs in epithelial cells in vivo.

Histological scanning of *ZO-3*$^{-/-}$ tissues. We examined various tissues of *ZO-3*$^{-/-}$ mice histologically at the light microscopic level using hematoxylin-eosin sections. In Fig. 4, hematoxylin-eosin sectional images are presented for the *ZO-3*$^{+/+}$ and *ZO-3*$^{-/-}$ lung, kidney, and liver. The ZO-3 deficiency did not appear to cause any histological changes in these *ZO-3*$^{-/-}$ tissues. In addition, we examined the histology of the *ZO-3*$^{-/-}$ heart, spleen, trachea, esophagus, stomach, small intestine, colon, brain, pancreas, spinal marrow, skin, thymus gland, suprarenal gland, pituitary gland, salivary gland, mammary gland, bladder, ovary, and bone and again detected no histological abnormalities (data not shown).

Generation of *ZO-3*-deficient F9 cells. To examine the function of ZO-3 at the cellular level in more detail, we attempted to establish *ZO-3*-deficient F9 cells. F9 is a clonal embryonal carcinoma cell line established from mouse teratocarcinoma. When F9 cells are suspension cultured to form cell aggregates in the presence of retinoic acid, cells delineating the surface of the aggregates differentiate into epithelial cells (visceral endodermal cells) (18). Therefore, F9 cells provide a good in vitro model system for the study of epithelial differentiation and morphogenesis.

In order to disrupt the two alleles of the *ZO-3* gene, we used two distinct types of targeting vectors (Fig. 5A). Targeting vector I, which was designed for the targeting of the *ZO-3* gene in ES cells, was used for targeting the first allele of the *ZO-3* gene of F9 cells. Of 1,000 neomycin-resistant clones examined, one clone (*ZO*$^{+/-}$ cells) had undergone a single homologous recombination as revealed by Southern blotting with 3′probe-1 (Fig. 5B). Then, to restore the sensitivity to neomycin in *ZO*$^{+/-}$ cells, the PGK-Neo cassette flanked by two loxP sequences in the first-targeted allele was removed by transfecting *ZO*$^{+/-}$ cells with the expression vector for Cre-recombinase (pCRE-PAC) (47) to obtain *ZO-3*$^{+/-}$ Cre cells (Fig. 5). For the second targeting of the *ZO-3* gene in *ZO*$^{+/-}$ Cre cells, targeting vector II was designed with the expectation that the targeting cassette would be inserted into exon 3 and that the second targeting would occur selectively to the yet-to-be-targeted wild-type allele of the *ZO-3* gene. The correct targeting of the second allele by targeting vector II was validated by Southern blotting with 3′probe-2 (Fig. 5).

Importantly, although targeting by targeting vector I completely removes coding regions from the *ZO-3* gene, targeting vector II simply intercalates the targeting cassette into exon 3. Thus, some sort of transcript might well be generated from the

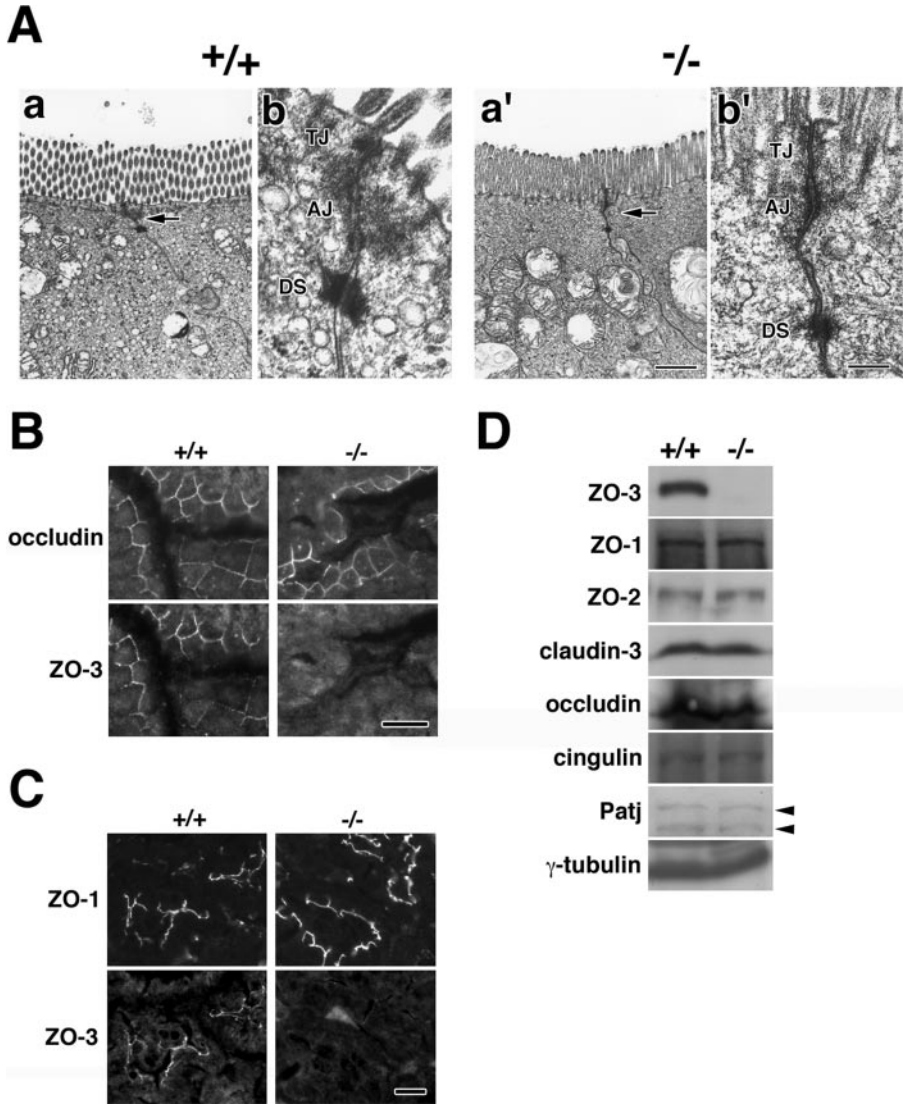

FIG. 3. TJs in *ZO-3*$^{-/-}$ mice. (A) Ultrathin-section electron microscopy. Both *ZO-3*$^{+/+}$ (+/+) and *ZO-3*$^{-/-}$ (−/−) intestinal epithelial cells are well polarized, bearing characteristic microvilli on their apical surface (a and a′) and well-developed junctional complexes at the most apical part of the lateral membranes (arrows). These junctional complexes are composed of TJs, AJs, and desmosomes (DS) as shown at the higher magnification (b and b′). Bars, 1 μm (a and a′) and 200 nm (b and b′). (B) Immunofluorescence microscopy of frozen sections of the *ZO-3*$^{+/+}$ (+/+) and *ZO-3*$^{-/-}$ (−/−) small intestine with antioccludin MAb and anti-ZO-3 PAb. Occludin is concentrated at the TJs irrespective of the occurrence of ZO-3. Bar, 10 μm. (C) Immunofluorescence microscopy of frozen sections of the *ZO-3*$^{+/+}$ (+/+) and *ZO-3*$^{-/-}$ (−/−) kidney with anti-ZO-1 PAb and anti-ZO-3 MAb. ZO-1 is localized normally at TJs of renal tubules in *ZO-3*$^{-/-}$ mice. Bar, 10 μm. (D) Immunoblotting of lysates of kidney of *ZO-3*$^{+/+}$ (+/+) and *ZO-3*$^{-/-}$ (−/−) mice with anti-ZO-3 PAb, anti-ZO-1 PAb, anti-ZO-2 PAb, anti-claudin-3 PAb, antioccludin MAb, anticingulin MAb, anti-Patj PAb, and anti-γ-tubulin MAb. The expression of ZO-3 was absent in the *ZO-3*$^{-/-}$ kidney, whereas the expression levels of other junction-associated proteins were indistinguishable between *ZO-3*$^{+/+}$ and *ZO-3*$^{-/-}$ kidneys. Blotting for γ-tubulin was used as a loading control.

targeting vector II-targeted allele. We suggest it to be a full-length ZO-3 mRNA in which the targeting cassette sequence is inserted, because the targeting cassette does not include a poly(A) signal sequence that provides the end of the transcript. To examine whether such a transcript is indeed expressed, we performed RT-PCR utilizing set of primers that correspond to the sequences within exon 2 and the targeting cassette of targeting vector II. In agreement with our prediction, a single PCR product was obtained only from the *ZO-3*$^{-/-}$ cells, in which targeting vector II was targeted (see Fig. S1A in the supplemental material). Surprisingly, sequencing analysis of this fragment revealed that splicing between exon 2 and exon 3 did not actually occur and the intron sequence was retained in the transcript (see Fig. S1B in the supplemental material). It may be that the targeting cassette sequence somehow interfered with the splicing between exon 2 and exon 3 because the insertion occurred in the vicinity of the splicing acceptor site of exon 3 (Fig. 5A; see also Fig. S1B in the supplemental material). Importantly, because an artificial in-frame stop codon (TGA) existed within this intron, the targeting vector-II tar-

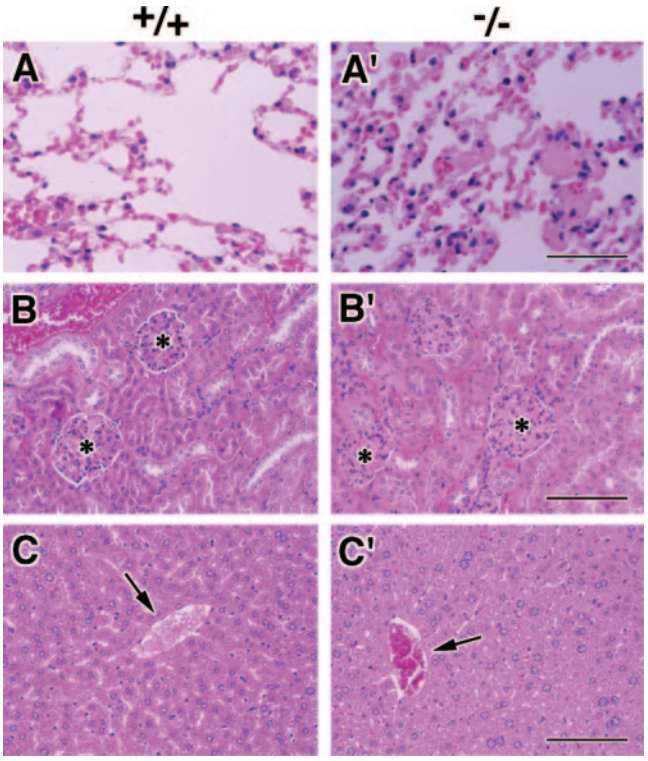

FIG. 4. Hematoxylin-eosin-stained sectional images of the lungs (A and A′), kidneys (B and B′), and livers (C and C′) of *ZO-3*$^{+/+}$ (+/+) and *ZO-3*$^{-/-}$ (−/−) mice. In all tissues examined, no significant abnormalities were found in *ZO-3*$^{-/-}$ mice. Asterisks, glomeruli; arrows, central veins. Bars, 50 μm (A and A′), 100 μm (B, B′, C, and C′).

geted allele would generate a very short peptide that is composed of the NH_2-terminal 15-amino-acid sequence of ZO-3 and two artificial amino acids (see Fig. S1B in the supplemental material). Because this peptide lacks any functional domains of ZO-3 (i.e., it contains merely the first six amino acids of the first PDZ domain of ZO-3), it should be nonfunctional. Therefore, it is likely that any functional ZO-3 is lost in our *ZO-3*$^{-/-}$ cells. If our prediction is correct (i.e., the targeted allele transcribes a full-length ZO-3 mRNA in which the targeting cassette is inserted), however, then the COOH-terminal coding region should also be detected by RT-PCR. Indeed, RT-PCR analysis utilizing a set of primers that correspond to the sequences within exon 4 and exon 5 (just downstream of the targeting cassette insertion site) or within exon 18 and exon 21 (extreme COOH-terminal part of the coding region) detected such a transcript, although its expression level appeared to be considerably low in *ZO-3*$^{-/-}$ cells (see Fig. S1C in the supplemental material). Because this region should be located downstream of the artificial stop codon described above, it is most likely not translated into a protein. If this region should be translated into a protein, however, it might retain some functions of ZO-3 because a large part of the functional domains of ZO-3 is encoded within this region. Such translation would occur if this region is a part of a transcript in which exon 2 is connected not with exon 3 but with some other downstream exons by an accidental splicing or in which an in-frame ATG codon within the targeting cassette or within the native exon of the gene was accidentally used as a start site of transcription. We found that such a translation did not actually occur, however, because immunoblotting, as well as immunostaining, of *ZO-3*$^{-/-}$ F9 cells utilizing two types of anti-ZO-3 antibodies, both of which were raised using the COOH terminus of ZO-3 (i.e., the region encoded from exon 18 to exon 21 of the *ZO-3* gene [amino acids 758 to 905 of mouse ZO-3]) as antigens, did not detect any positive signals (Fig. 6B and C; see also Fig. S1D in the supplemental material). Taken all together, we conclude that no functional ZO-3 is expressed in our *ZO-3*$^{-/-}$ F9 cells.

TJ proteins in *ZO-3*$^{-/-}$ F9 cells. Close examination of *ZO-3*$^{-/-}$ mice detected no histological or physiological abnormalities, indicating that ZO-3 is dispensable for the morphogenesis and functions of the epithelium, especially of TJs, at least in the laboratory environment. Therefore, it is reasonable to speculate that some TJ component is upregulated to compensate for the deficiency of ZO-3 in TJs. It is also possible that some component is downregulated at TJs in the absence of ZO-3. To discuss these points, an analysis with chimeric aggregates of *ZO-3*$^{+/+}$ and *ZO-3*$^{-/-}$ F9 cells is needed. Prior to performing such an analysis, however, we checked whether *ZO-3*$^{-/-}$ F9 cells differentiate normally into visceral endodermal epithelium-like cells. When *ZO-3*$^{-/-}$ F9 cells were suspension cultured in the presence of retinoic acid, so-called embryoid bodies were formed, which were indistinguishable in appearance and size from the wild-type ones (Fig. 6Aa and a′). Ultrathin-section electron microscopy identified visceral endodermal cells with a normal appearance delineating the outer surface of *ZO-3*$^{-/-}$ embryoid bodies, and these cells bore normal junctional complexes between adjacent cells, although in these, as well as wild-type cells, the TJs were not clearly sorted out from AJs (Fig. 6Ab, c, b′, and c′). To examine their differentiation at the molecular level, we then checked the expression levels of several junctional proteins by immunoblotting. Several genes have been reported to have an altered expression in F9 cells induced to undergo differentiation by retinoic acid (27). We here found that several junctional proteins, including ZO-3, were upregulated when cultured in the presence of retinoic acid in wild-type cells, although the expression of ZO-1 was not significantly affected (Fig. 6B, +/+). Importantly, a similar expression pattern was found in *ZO-3*$^{-/-}$ cell aggregates except that ZO-3 was not expressed (Fig. 6B, −/−). Taken together, differentiation, even in the absence of ZO-3 expression, appeared to occur normally at the morphological and molecular levels.

We then examined the molecular architecture of TJs of *ZO-3*$^{-/-}$ epithelial cells by immunostaining. For this purpose, we formed chimeric aggregates by coculturing the mixture of wild-type and *ZO-3*$^{-/-}$ F9 cells, and these aggregates were whole mount stained doubly with anti-ZO-3 antibody and another antibody for a given TJ component. Through this type of analysis, we can precisely evaluate the effects of the *ZO-3* deficiency on other TJ components by immunofluorescence microscopy (Fig. 6C). First, we examined the behavior of ZO-1 and ZO-2 in *ZO-3*$^{-/-}$ cells. When chimeric aggregates were double stained with anti-ZO-1 PAb and anti-ZO-3 MAb, the degree to which ZO-1 concentrated at TJs appeared to be independent of the presence or absence of ZO-3 (Fig. 6Ca). In contrast, interestingly, ZO-2 appeared to be concentrated at

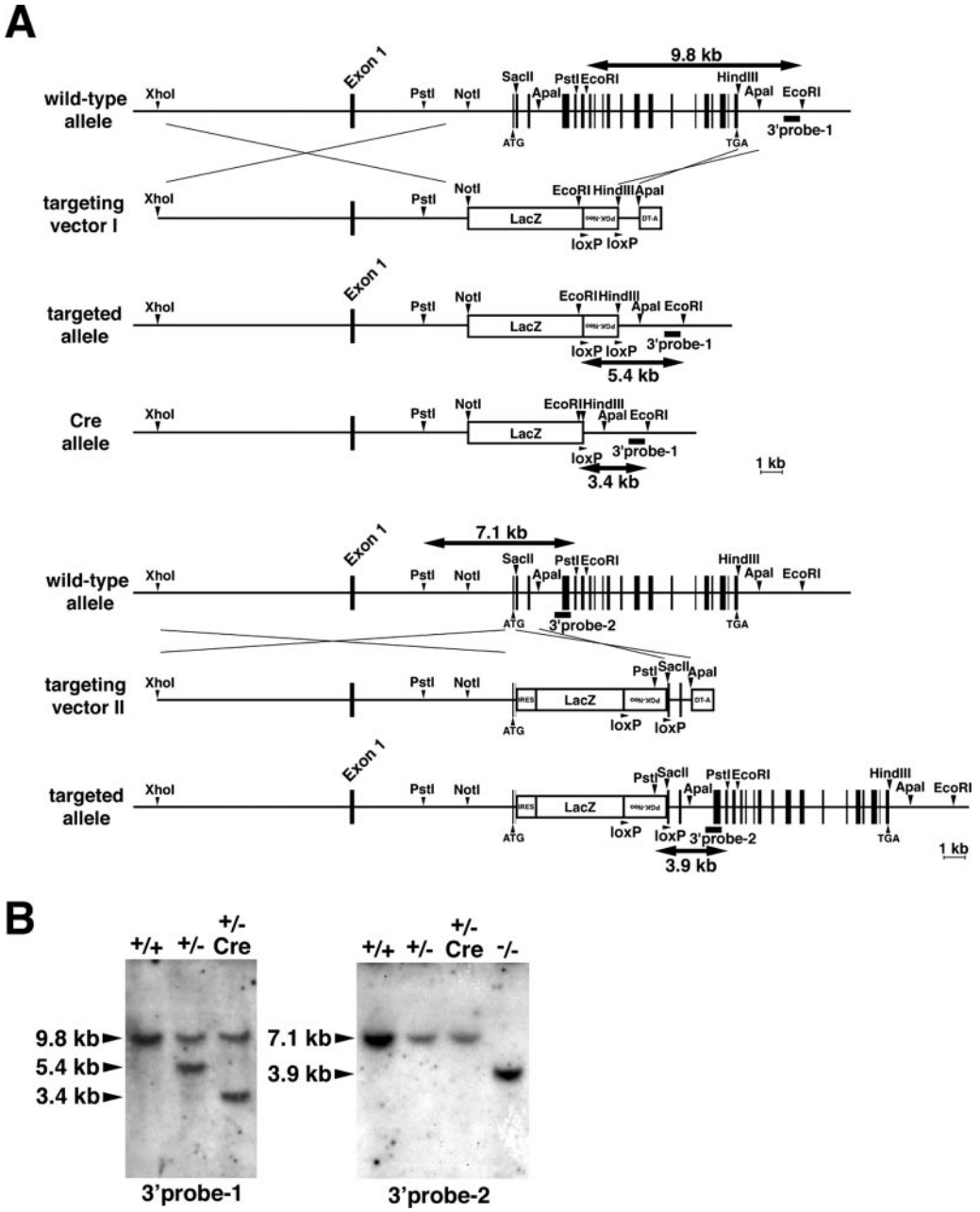

FIG. 5. Generation of *ZO-3*$^{-/-}$ F9 cells. (A) Restriction maps of the wild-type allele, the first and second targeting vectors (targeting vector I and II), the Cre-treated allele (Cre allele), and the targeted alleles of the mouse *ZO-3* gene. Targeting vector I is the same as that used for the generation of *ZO-3*$^{-/-}$ mice (see Fig. 2A). Targeting vector II contained an IRES-LacZ/PGK-Neo cassette in the middle and DT-A cassette just on the 3′ side of the 3′ arm to insert the IRES-LacZ/PGK-Neo cassette into exon 3. The positions of 3′probe-1 and 3′probe-2 for Southern blotting are indicated by bars. (B) Genotype analyses by Southern blotting of EcoRI-digested (with 3′probe-1) and PstI-digested (with 3′probe-2) genomic DNA from wild-type (+/+), heterozygous (+/−), Cre-treated heterozygous (+/− Cre), and homozygous (−/−) F9 cells. Southern blotting with 3′probe-1 yielded a 9.8-kb band from the wild-type allele, a 5.4-kb band from the first targeted allele, and a 3.4-kb band from the Cre-treated allele. Southern blotting with 3′probe-2 yielded a 7.1-kb band from the wild-type allele, a 3.9-kb band from the second targeted allele, and no band from the first targeted and the Cre-treated alleles.

ZO-3-deficient TJs in a slightly larger amount than at wild-type TJs in many chimeric aggregates (Fig. 6Cb). To confirm this upregulation of ZO-2 in *ZO-3*-deficient TJs, we established a *ZO-3*$^{-/-}$ F9 cell line expressing exogenous ZO-3 and formed chimeric aggregates between this cell line and *ZO-3*$^{-/-}$ F9 cells (Fig. 6Cc). Whole-mount immunostaining with anti-ZO-2 PAb revealed that the exogenous expression of ZO-3 in *ZO-3*$^{-/-}$ visceral endodermal cells decreased the concentration of ZO-2 at TJs down to the wild-type level. Using the chimeric aggregates, we next examined the behavior of three TJ integral membrane proteins—occludin, JAM1, and claudins (claudin-3 and -4)—in *ZO-3*$^{-/-}$ visceral endodermal cells, but none of

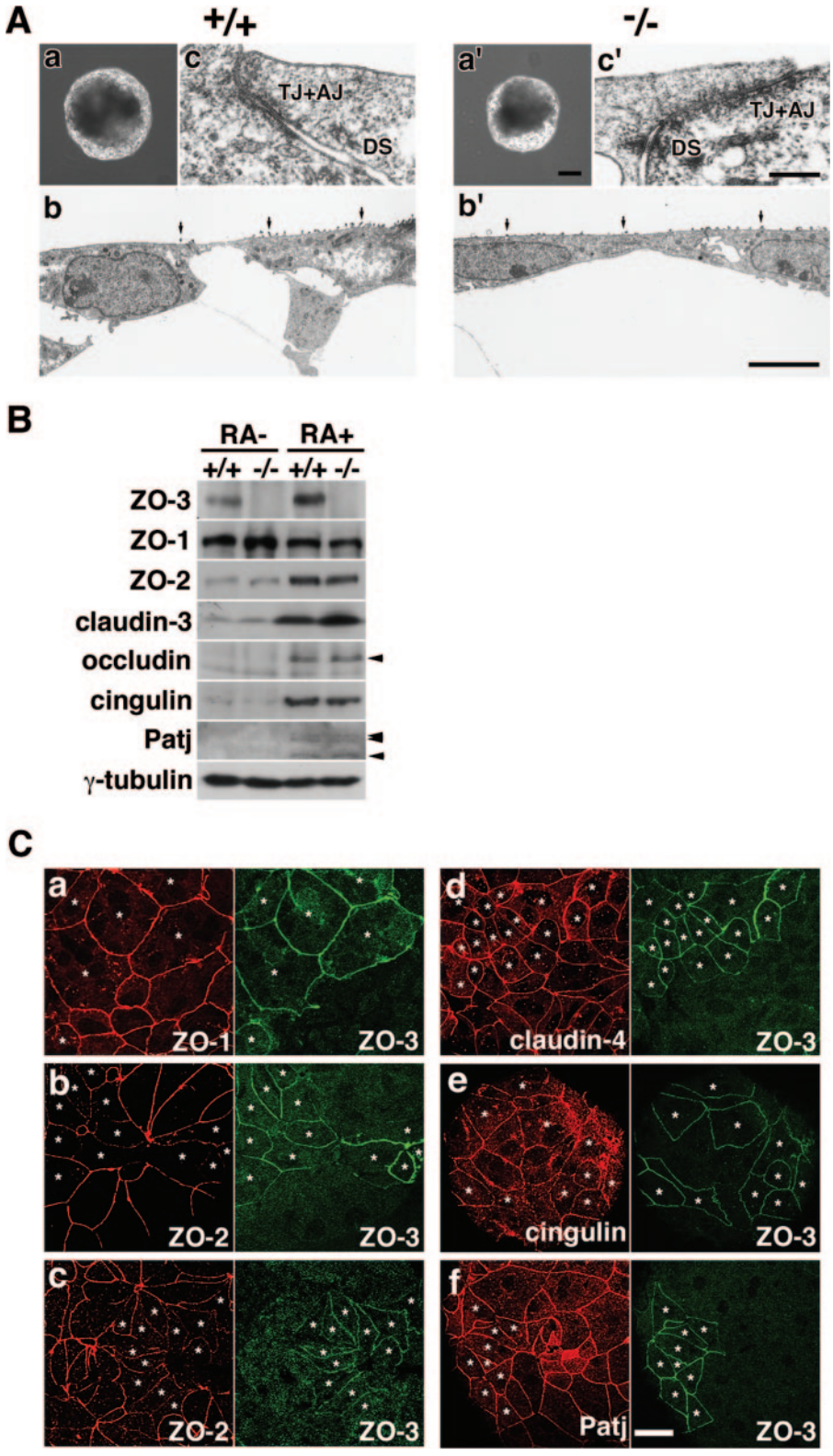

FIG. 6. Phenotypic analyses of the visceral endoderm differentiated from *ZO-3*$^{+/+}$ and *ZO-3*$^{-/-}$ F9 cells. (A) Morphology of *ZO-3*$^{+/+}$ (+/+) and *ZO-3*$^{-/-}$ (−/−) F9 cell aggregates. Phase-contrast microscopy (a and a′) showed that *ZO-3*$^{+/+}$ and *ZO-3*$^{-/-}$ cell aggregates were similar in size and appearance. Ultrathin-section electron microscopy (b and b′) revealed at low magnification that both *ZO-3*$^{+/+}$ and *ZO-3*$^{-/-}$ cells delineating the outer surface of cell aggregates (visceral endodermal cells) were polarized with short microvilli on their apical surface (arrows). At higher magnification (c and c′), cell-cell contact sites of *ZO-3*$^{+/+}$ and *ZO-3*$^{-/-}$ visceral endodermal cells were characterized by junctional complexes consisting of TJs, AJs, and desmosomes (DS). Bars: 100 μm (a and a′), 5 μm (b and b′), 200 nm (c and c′). (B) Immunoblotting of whole-cell lysates of *ZO-3*$^{+/+}$ (+/+) and *ZO-3*$^{-/-}$ (−/−) F9 cell aggregates that are cultured for 6 days in the presence (RA+) or absence (RA−)

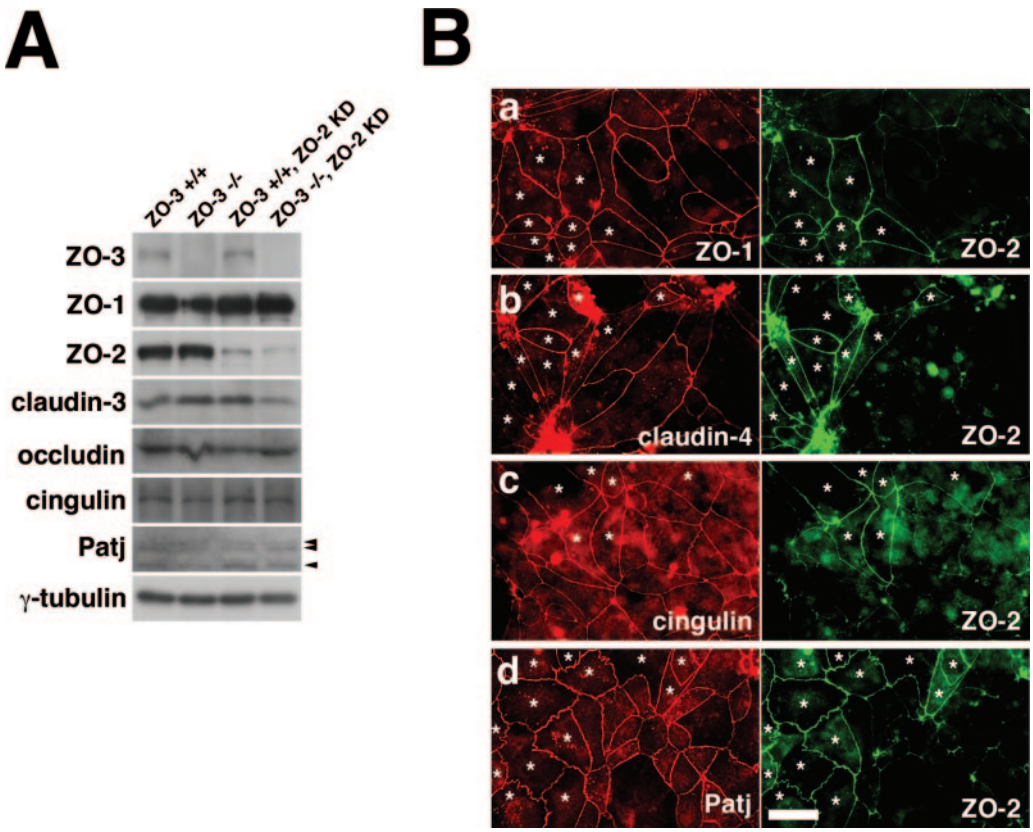

FIG. 7. Phenotypic analyses of F9 cells lacking the expression of ZO-3 and ZO-2 differentiated under monolayer culture conditions. (A) Immunoblotting of whole-cell lysates of *ZO-3*$^{+/+}$, *ZO-3*$^{-/-}$, *ZO-3*$^{+/+}$/*ZO-2*^{KD} and *ZO-3*$^{-/-}$/*ZO-2*^{KD} F9 cells that are cultured for 7 days in the presence of retinoic acid under monolayer culture conditions. Each of the lysates was blotted with anti-ZO-3 PAb, anti-ZO-1 PAb, anti-ZO-2 PAb, anti-claudin-3 PAb, antioccludin MAb, anticingulin MAb, anti-Patj PAb, and anti-γ-tubulin MAb. Expression patterns of several junctional proteins were indistinguishable among these four cells, except that ZO-3 expression disappeared in *ZO-3*$^{-/-}$ and *ZO-3*$^{-/-}$/*ZO-2*^{KD} cells and that ZO-2 expression was suppressed in *ZO-3*$^{+/+}$/*ZO-2*^{KD} and *ZO-3*$^{-/-}$/*ZO-2*^{KD} cells. Blotting for γ-tubulin was used as a loading control. (B) Immunostaining of chimeric cell monolayers formed by coculturing a mixture of *ZO-3*$^{-/-}$ and *ZO-3*$^{-/-}$/*ZO-2*^{KD} cells. These chimeric aggregates were doubly stained with anti-ZO-1 MAb–anti-ZO-2 PAb (a), anti-claudin-4 MAb–anti-ZO-2 PAb (b), anticingulin MAb–anti-ZO-2 PAb (c), or anti-Patj PAb–anti-ZO-2 MAb (d). *ZO-3*$^{-/-}$ cells are indicated by asterisks. The concentration of ZO-1, claudin-4, cingulin, and Patj does not appear to differ between ZO-2-positive and ZO-2-negative TJs with the *ZO-3*$^{-/-}$ background. Bar, 20 μm.

them appeared to be affected in their distribution or concentration at TJs by the ZO-3 deficiency (Fig. 6Cd and data not shown). Finally, we examined two other TJ plaque proteins in *ZO-3*$^{-/-}$ visceral endodermal cells: cingulin and Patj. We previously showed that cingulin disappeared from TJs in ZO-1-deficient epithelial cells (52), but cingulin was normally concentrated at TJs in the absence of ZO-3 (Fig. 6Ce). Patj is believed to be involved in the establishment of epithelial polarity, and ZO-3 was suggested to contribute to the localization of Patj to TJs by directly binding to Patj (40). However, Patj appeared to be normally recruited to TJs in *ZO-3*$^{-/-}$ visceral endodermal cells (Fig. 6Cf).

Examination of possible functional compensation by ZO-2. We found no apparent abnormalities at TJs in *ZO-3*$^{-/-}$ F9 cells except for the upregulation of ZO-2. Because ZO-2 has significant structural similarities with ZO-3, there arises a possibility that ZO-2 compensates for the function of ZO-3 at ZO-3-deficient TJs. To examine this, we stably knocked down

of retinoic acid. Each of the whole-cell lysates was blotted with anti-ZO-3 PAb, anti-ZO-1 PAb, anti-ZO-2 PAb, anti-claudin-3 PAb, antioccludin MAb, anti-cingulin MAb, anti-Patj PAb, and anti-γ-tubulin MAb. Retinoic acid affected the expression levels of many junctional proteins, and their expression patterns were indistinguishable between *ZO-3*$^{+/+}$ and *ZO-3*$^{-/-}$ cells except that the expression of ZO-3 disappeared in *ZO-3*$^{-/-}$ cells. Blotting for γ-tubulin was used as a loading control. (C) Immunostaining of chimeric cell aggregates formed by coculturing a mixture of *ZO-3*$^{+/+}$ and *ZO-3*$^{-/-}$ cells (a, b, d, e, and f) or a mixture of *ZO-3*$^{-/-}$ cells exogenously expressing ZO-3 (*ZO-3*$^{-/-/+}$ cells) and *ZO-3*$^{-/-}$ cells (c). These chimeric aggregates were whole-mount stained doubly with anti-ZO-1 MAb–anti-ZO-3 PAb (a), anti-ZO-2 PAb–anti-ZO-3 MAb (b and c), anti-claudin-4 MAb–anti-ZO-3 PAb (d), anticingulin MAb–anti-ZO-3 PAb (e), or anti-Patj PAb–anti-ZO-3 MAb (f). *ZO-3*$^{+/+}$ cells and *ZO-3*$^{-/-/+}$ cells are marked by asterisks. The concentrations of ZO-1, claudin-4, cingulin, and Patj do not appear to differ between ZO-3-positive and ZO-3-negative TJs (a, d, e, and f). Note that ZO-2 is concentrated in a significantly larger amount at ZO-3-negative TJs between adjacent *ZO-3*$^{-/-}$ cells than ZO-3-positive TJs between *ZO-3*$^{+/+}$ cells (b) or *ZO-3*$^{-/-/+}$ cells (c). Bar, 20 μm.

the expression of ZO-2 in *ZO-3*$^{-/-}$ F9 cells by RNA interference. These cells are referred to as *ZO-3*$^{-/-}$/*ZO-2*^{KD} cells. As a control, the expression of ZO-2 was also knocked down in wild-type F9 cells to obtain *ZO-3*$^{+/+}$/*ZO-2*^{KD} cells. Although epithelial differentiation of F9 cells induced by retinoic acid is usually observed when they are cultured in suspension to form cell aggregates as described above, differentiation could also be substantially attained under monolayer culture conditions (27). Then, *ZO-3*$^{+/+}$/*ZO-2*^{KD} and *ZO-3*$^{-/-}$/*ZO-2*^{KD} cells, together with wild-type (*ZO-3*$^{+/+}$) and *ZO-3*$^{-/-}$ cells, were cultured in the presence of retinoic acid under monolayer conditions. Immunoblotting of their lysates has shown that the expression of ZO-2 was suppressed by ca. 90% in both *ZO-3*$^{+/+}$/*ZO-2*^{KD} and *ZO-3*$^{-/-}$/*ZO-2*^{KD} cells, showing that RNA interference was effective (Fig. 7A). Of significant importance, the expression levels of several other junctional proteins were mostly indistinguishable among these four types of cells. This result suggests that epithelial differentiation can be comparably achieved even in the absence of ZO-3, ZO-2, or both. Then, in order to examine whether ZO-2 compensates for *ZO-3* deficiency at *ZO-3*$^{-/-}$ TJs, we made chimeric monolayer cultures by coculturing *ZO-3*$^{-/-}$ and *ZO-3*$^{-/-}$/*ZO-2*^{KD} cells. Thus, if the normal molecular architecture of TJs in *ZO-3*$^{-/-}$ cells is due to a compensatory role of ZO-2, then some abnormalities will be apparent on the loss of ZO-2 in *ZO-3*$^{-/-}$ cells (i.e., *ZO-3*$^{-/-}$/*ZO-2*^{KD} cells). Significantly, we found that the degree to which ZO-1 concentrated at TJs is indistinguishable between *ZO-3*$^{-/-}$ and *ZO-3*$^{-/-}$/*ZO-2*^{KD} cells (Fig. 7B). Moreover, the behaviors of three other TJ proteins, claudin-4, cingulin, and Patj, was also indistinguishable in terms of their distribution and concentration at TJs (Fig. 7B). These results suggest that *ZO-3*$^{-/-}$ cells have normal TJs not because ZO-2 compensates for ZO-3, but because ZO-3 actually does not have any role in the molecular architecture of TJs, at least in our experimental conditions. In other words, these results imply that TJs can be normally established in the concomitant absence of ZO-2 and ZO-3.

Examination of possible roles of ZO-3 in the formation of TJs. Although we could not find any role for ZO-3 in terms of the molecular architecture of TJs, it has been well documented that many proteins do not affect steady-state TJs but affect the process of TJ formation. Then, to examine the possible roles of ZO-3 in the process of TJ formation, a Ca^{2+} switch assay was performed. In this experiment, F9 cells differentiated under monolayer culture conditions were cultured overnight in a low-Ca^{2+} medium containing 5 μM Ca^{2+}, so that their cell-cell junctions are completely disrupted. Then, the medium was switched to a normal medium to initiate the reassembly of the junctions ("Ca^{2+} switch"), and the process was followed.

Because the formation of TJs is always dependent on the formation of AJs (38, 46, 48), we first examined the formation of E-cadherin-positive AJs. As shown in Fig. 8A, in wild-type (*ZO-3*$^{+/+}$) cells E-cadherin-positive primordial cell-cell junctions begin to form at 0.5 h after the transfer of the medium. They then gradually grew to be aligned in a linear fashion more densely, and the process was mostly completed to develop continuous AJs at 4 h. Significantly, the time course of E-cadherin-positive AJ formation of *ZO-3*$^{-/-}$ cells was indistinguishable from that of *ZO-3*$^{+/+}$ cells. Moreover, *ZO-3*$^{-/-}$/*ZO-2*^{KD} cells also had an ability to assemble E-cadherin-positive AJs with a comparable time course. Thus, the speed of AJ formation is not affected by the presence or absence of ZO-3 or by the presence or absence of both ZO-3 and ZO-2.

In the process of cell-cell junction formation, E-cadherin and ZO-1 first colocalized at primordial spot-like junctions, but they gradually separated to form AJs and TJs, respectively (2). We then examined the distribution of ZO-1 in our Ca^{2+} switch experiment. As shown in Fig. 8B, in wild-type *ZO-3*$^{+/+}$ cells the time course of ZO-1-positive junction formation was quite similar to that of E-cadherin-positive junctions, where ZO-1-positive junctions are apparent at 0.5 h and almost completely formed at 2 to 4 h. Again, this time course is indistinguishable in *ZO-3*$^{-/-}$ cells, as well as in *ZO-3*$^{-/-}$/*ZO-2*^{KD} cells. The accumulation of other TJ-associated proteins, including JAM1, cingulin, Par6, and Patj, was also examined. However, these molecules also normally assembled at the TJs of *ZO-3*$^{-/-}$ cells or *ZO-3*$^{-/-}$/*ZO-2*^{KD} cells, although the time course differed depending on the molecules examined (Fig. 8C and data not shown). As for Patj, for example, considerable TJ localization was apparent at around 1 h and was completed at 4 h or later (Fig. 8C). Thus, ZO-3 seems to be dispensable not only for the molecular architecture of TJs but also for the speed of TJ formation. Moreover, functional compensation of ZO-3 by ZO-2 is unlikely in this process.

DISCUSSION

Although ZO-1 and ZO-2 are expressed not only in endothelia and epithelia but also in a wide variety of tissues, ZO-3 is exclusively expressed in epithelial cells. Thus, ZO-3 was suggested to have some important roles specifically at the TJs of epithelial cells. It was therefore surprising that the *ZO-3* deficiency did not result in any significant abnormalities at the whole body or the cellular level. *ZO-3*$^{-/-}$ mice were viable and fertile, and their epithelia possessed well-organized TJs, indicating that ZO-3 is not required for the normal development or survival of mice in the laboratory environment. Moreover, *ZO-3*$^{-/-}$ F9 cells differentiated into epithelial cells normally in the presence of retinoic acid, and these epithelial cells bore TJs with a normal appearance and molecular architecture. A Ca^{2+} switch experiment has shown that ZO-3 is not responsible for the process of TJ formation either.

What, then, is the physiological function of ZO-3? It is possible that its real function has been overlooked in mice grown in the laboratory environment. For example, the possibility cannot be excluded that ZO-3 is indispensable for some pathological events such as certain defense mechanisms of epithelial cells against microorganisms. Another possibility is, of course, that the TJ MAGUKs—ZO-1, ZO-2, and ZO-3—are functionally redundant and that ZO-1 and/or ZO-2 functionally compensate for the lack of ZO-3 not only at the whole body but also at the cellular level. Indeed, these three proteins shared significant structural similarities, which is the reason why they are collectively called MAGUKs. Thus, it is important to closely consider the molecular relationships between these three TJ MAGUKs. ZO-1, ZO-2, and ZO-3 were all reported to directly bind to the COOH termini of claudins at their PDZ1 domains (13, 17, 21, 22, 53). At least in vitro, ZO-1 forms a heterodimeric complex with ZO-2 or ZO-3 through PDZ2-PDZ2 interaction (21), but ZO-2 does not bind to

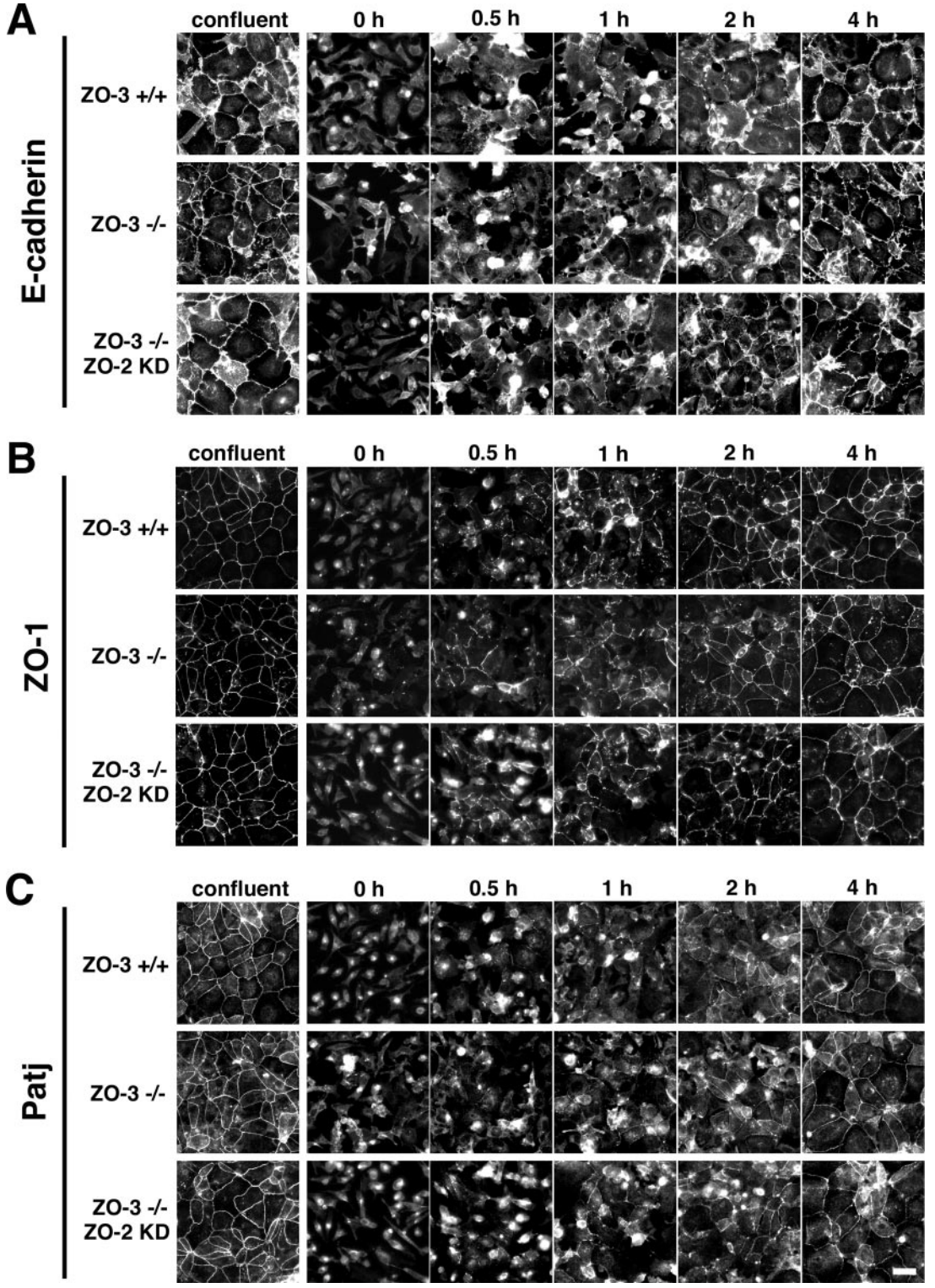

FIG. 8. Ca^{2+} switch experiment. *ZO-3*$^{+/+}$, *ZO-3*$^{-/-}$, and *ZO-3*$^{-/-}$/*ZO-2*^{KD} cells were cultured under monolayer conditions in the presence of retinoic acid for 7 days. They were then cultured in a low Ca^{2+} medium containing 5 μM Ca^{2+} overnight and were transferred to a normal culture medium. After 0.5, 1, 2, and 4 h of incubation, cells were fixed and stained with anti-E-cadherin MAb (A), anti-ZO-1 MAb (B), or anti-Patj PAb (C). Junction formation similarly proceeded in *ZO-3*$^{+/+}$, *ZO-3*$^{-/-}$, and *ZO-3*$^{-/-}$/*ZO-2*^{KD} cells. Bar, 20 μm.

ZO-3. If this is the case also in vivo, it is speculated that ZO-1 has its own specific function and that ZO-2 and ZO-3 are functionally redundant. Consistent with such a contention, in *ZO-3*$^{-/-}$ visceral endodermal cells the concentration of ZO-2 was increased slightly but significantly at TJs. Furthermore, our studies with *ZO-1*-deficient Eph4 epithelial cells revealed that ZO-1 and ZO-2 are not necessarily functionally redundant. Thus, in *ZO-1*$^{-/-}$ Eph4 cells, the formation of TJs was retarded after a Ca^{2+} switch, and cingulin disappeared from TJs, and these phenotypic changes were rescued by the exogenous expression of ZO-1 but not by that of ZO-2, indicating that ZO-1 has its own specific functions (52). Therefore, it can be speculated that the lack of abnormalities in TJs of *ZO-3*$^{-/-}$ mice and F9 cells is due to the functional compensation of ZO-2 for the ZO-3 deficiency. However, we found that suppression of ZO-2 expression by RNA interference did not affect the TJ architecture in *ZO-3*$^{-/-}$ F9 cells. It might be that a trace amount of residual ZO-2 was sufficient to rescue ZO-3 function. More likely, however, is that ZO-3 indeed has no particular molecular functions at least in the normal laboratory environment. Several observations support this assumption. (i) A Ca^{2+} switch experiment has shown that the loss of ZO-3 did not even affect the process of TJ formation. (ii) Cultured mouse Eph4 epithelial cells originally express only a negligible amount of ZO-3 but have a normal epithelial morphology with well-established TJs (20, 51, 52). (iii) In both Eph4 cells and F9 cells, the concomitant suppression of ZO-1 and ZO-2 sufficiently disrupted the TJ structure (51). (iv) Exogenous expression of either ZO-1 or ZO-2 in *ZO-1*/*ZO-2*-deficient Eph4 cells, where all three TJ MAGUKs are substantially lost, successively rescued the TJ structure, whereas that of ZO-3 did not (51). Thus, among three homologous TJ MAGUKs, ZO-3 is the only molecule that does not have an ability to polymerize TJ strands by itself. Taken together, these observations show that, unlike ZO-1 and ZO-2, ZO-3 appears to have no physiological functions that are apparent under normal laboratory conditions.

Finally, we should discuss two TJ plaque proteins, cingulin and Patj, that were reported to be localized at TJs and to directly bind to ZO-3 (9, 17, 21, 40, 53). Our observations here clearly showed that the localization of these proteins is not dependent on ZO-2 or ZO-3. Taken together, with our previous analyses of *ZO-1*$^{-/-}$ Eph4 cells (52), we can conclude that cingulin is recruited to TJs through its binding to ZO-1, not to ZO-2 or ZO-3. Patj, which is thought to be directly involved in the epithelial polarization, was reported to directly bind to the COOH terminus of ZO-3 through its PDZ6 domain, and Patj was shown to lose its ability to localize at TJs when its PDZ6 domain was deleted (40). It has not been shown that Patj binds to ZO-1 or ZO-2 directly. Through these findings, it was assumed that ZO-3 is indispensable for the localization of Patj at TJs, but the present findings clearly do not support this assumption. Since Patj binds to several TJ-associated molecules other than ZO-3 such as Pals1 and Par6 (35, 41), it would be reasonable to speculate that in the absence of ZO-3, Patj is recruited to TJs through its binding to these proteins. Indeed, both Pals1 and Par6 were normally concentrated at TJs in *ZO-3*$^{-/-}$ visceral endodermal cells (not shown).

The present study did not clarify the specific functions of ZO-3 at either the whole-body level or the cellular level. Further generation of mutant mice lacking the TJ MAGUKs ZO-1, -2, and -3, both singly and in combination, will lead to a better understanding of the physiological relevance of the occurrence of these three closely related proteins at TJs.

ACKNOWLEDGMENTS

We thank all members of our laboratory for helpful discussions. We also thank Takeshi Matsui for helpful suggestions.

This study was supported in part by a Grant-in-Aid for Cancer Research and a Grant-in-Aid for Scientific Research from the Ministry of Education, Science, and Culture of Japan (to S.T.).

REFERENCES

1. **Anderson, J. M., and C. M. Van Itallie.** 1995. Tight junctions and the molecular basis for regulation of paracellular permeability. Am. J. Physiol. **269:**G467–G475.
2. **Ando-Akatsuka, Y., S. Yonemura, M. Itoh, M. Furuse, and S. Tsukita.** 1999. Differential behavior of E-cadherin and occludin in their colocalization with ZO-1 during the establishment of epithelial cell polarity. J. Cell Physiol. **179:**115–125.
3. **Balda, M. S., L. González-Mariscal, K. Matter, M. Cereijido, and J. M. Anderson.** 1993. Assembly of the tight junction: the role of diacylglycerol. J. Cell Biol. **123:**293–302.
4. **Balda, M. S., and K. Matter.** 1998. Tight junctions. J. Cell Sci. **111:**541–547.
5. **Balda, M. S., and K. Matter.** 2000. The tight junction protein ZO-1 and an interacting transcription factor regulate ErbB-2 expression. EMBO J. **19:** 2024–2033.
6. **Benais-Pont, G., A. Punn, C. Flores-Maldonado, J. Eckert, G. Raposo, T. P. Fleming, M. Cereijido, M. S. Balda, and K. Matter.** 2003. Identification of a tight junction-associated guanine nucleotide exchange factor that activates Rho and regulates paracellular permeability. J. Cell Biol. **160:**729–740.
7. **Citi, S., H. Sabanay, R. Jakes, B. Geiger, and J. Kendrick-Jones.** 1988. Cingulin, a new peripheral component of tight junctions. Nature **333:**272–276.
8. **Cohen, C. J., J. Y. Shieh, R. J. Pickles, T. Okegawa, J. T. Hsieh, and J. M. Bergelson.** 2001. The coxsackievirus and adenovirus receptor is a transmembrane component of the tight junction. Proc. Natl. Acad. Sci. USA **98:**15191–15196.
9. **Cordenonsi, M., F. D'Atri, E. Hammar, D. A.D. Parry, J. Kendrick-Jones, D. Shore, and S. Citi.** 1999. Cingulin contains globular and coiled-coil domains and interacts with ZO-1, ZO-2, ZO-3 and myosin. J. Cell Biol. **147:**1569–1581.
10. **Farquhar, M. G., and G. E. Palade.** 1963. Junctional complexes in various epithelia. J. Cell Biol. **17:**375–412.
11. **Furuse, M., K. Fujita, T. Hiiragi, K. Fujimoto, and S. Tsukita.** 1998. Claudin-1 and -2: novel integral membranes proteins localizing at tight junctions with no sequence similarity to occludin. J. Cell Biol. **141:**1539–1550.
12. **Furuse, M., T. Hirase, M. Itoh, A. Nagafuchi, S. Yonemura, S. Tsukita, and S. Tsukita.** 1993. Occludin: a novel integral membrane protein localizing at tight junctions. J. Cell Biol. **123:**1777–1788.
13. **Furuse, M., M. Itoh, T. Hirase, A. Nagafuchi, S. Yonemura, S. Tsukita, and S. Tsukita.** 1994. Direct association of occludin with ZO-1 and its possible involvement in the localization of occludin at tight junctions. J. Cell Biol. **127:**1617–1626.
14. **González-Mariscal, L., A. Betanzos, and A. Ávila-Flores.** 2000. MAGUK proteins: structure and role in the tight junction. Semin. Cell Dev. Biol. **11:**315–324.
15. **Gumbiner, B., T. Lowenkopf, and D. Apatira.** 1991. Identification of a 160-kDa polypeptide that binds to the tight junction protein ZO-1. Proc. Natl. Acad. Sci. USA **88:**3460–3466.
16. **Hamazaki, Y., M. Itoh, H. sasaki, M. Furuse, and S. Tsukita.** 2002. Multi-PDZ domain protein 1 (MUPP1) is concentrated at tight junctions through its possible interaction with claudin-1 and junctional adhesion molecule. J. Biol. Chem. **277:**455–461.
17. **Haskins, J., L. Gu, E. S. Wittchen, J. Hibbard, and B. R. Stevenson.** 1998. ZO-3, a novel member of the MAGUK protein family found at the tight junction, interacts with ZO-1 and occludin. J. Cell Biol. **141:**199–208.
18. **Hogan, B. L., A. Taylor, and E. Adamson.** 1981. Cell interactions modulate embryonal carcinoma cell differentiation into parietal or visceral endoderm. Nature **291:**235–237.
19. **Ikenouchi, J., M. Furuse, K. Furuse, H. Sasaki, S. Tsukita, and S. Tsukita.** 2005. Tricellulin constitutes a novel barrier at tricellular contacts of epithelial cells. J. Cell Biol. **171:**939–945.
20. **Inoko, A., M. Itoh, A. Tamura, M. Matsuda, M. Furuse, and S. Tsukita.** 2003. Expression and distribution of ZO-3, a tight junction MAGUK protein, in mouse tissues. Genes Cells **8:**837–845.
21. **Itoh, M., M. Furuse, K. Morita, K. Kubota, M. Saitou, and S. Tsukita.** 1999. Direct binding of three tight junction-associated MAGUKs, ZO-1, ZO-2, and ZO-3, with the COOH termini of claudins. J. Cell Biol. **147:**1351–1363.

22. **Itoh, M., K. Morita, and S. Tsukita.** 1999. Characterization of ZO-2 as a MAGUK family member associated with tight as well as adherens junctions with a binding affinity to occludin and α catenin. J. Biol. Chem. **274:**5981–5986.
23. **Itoh, M., S. Yonemura, A. Nagafuchi, S. Tsukita, and S. Tsukita.** 1991. A 220-kD undercoat-constitutive protein: its specific localization at cadherin-based cell-cell adhesion sites. J. Cell Biol. **115:**1449–1462.
24. **Izumi, Y., T. Hirose, Y. Tamai, S. Hirai, Y. Nagashima, T. Fujimoto, Y. Tabuse, K. J. Kemphues, and S. Ohno.** 1998. An atypical PKC directly associates and colocalizes at the epithelial tight junction with ASIP, a mammalian homologue of *Caenorhabditis elegans* polarity protein PAR-3. J. Cell Biol. **143:**95–106.
25. **Joberty, G., C. Petersen, L. Gao, and I. G. Macara.** 2000. The cell-polarity protein Par6 links Par3 and atypical protein kinase C to Cdc42. Nat. Cell Biol. **2:**531–539.
26. **Johansson, A. S., M. Driessens, and P. Aspenström.** 2000. The mammalian homologue of the *Caenorhabditis elegans* polarity protein PAR-6 is a binding partner for the Rho GTPases Cdc42 and Rac1. J. Cell Sci. **133:**3267–3275.
27. **Komiya, S., M. Shimizu, J. Ikenouchi, S. Yonemura, T. Matsui, Y. Fukunaga, H. Liu, F. Endo, S. Tsukita, and A. Nagafuchi.** 2005. Apical membrane and junctional complex formation during simple epithelial cell differentiation of F9 cells. Genes Cells **10:**1065–1080.
28. **Lemmers. C., E. Médina, M. H. Delgrossi, D. Michel, J. P. Arsanto, and A. Le Bivic.** 2002. hINAD/PATJ, a homolog of Discs Lost, interacts with Crumbs and localizes to tight junction in human epithelial cells. J. Biol. Chem. **277:**25408–25415.
29. **Lin, D., A. S. Edwards, J. P. Fawcett, G. Mbamalu, J. D. Scott, and T. Pawson.** 2000. A mammalian PAR-3-PAR-6 complex implicated in Cdc42/Rac1 and aPKC signalling and cell polarity. Nat. Cell Biol. **2:**540–547.
30. **Maeno, Y., S. Moroi, H. Nagashima, T. Noda, H. Shiozaki, M. Monden, S. Tsukita, and A. Nagafuchi.** 1999. α-catenin-deficient F9 cells differentiate into signet ring cells. Am. J. Pathol. **154:**1323–1328.
31. **Makarova, O., M. H. Roh, C. J. Liu, S. Laurinec, and B. Margolis.** 2003. Mammalian Crumbs3 is a small transmembrane protein linked to protein associated with Lin-7 (Pals1). Gene **302:**21–29.
32. **Martin-Padura, I., S. Lostaglio, M. Schneemann, L. Williams, M. Romano, P. Fruscella, C. Panzeri, A. Stoppacciaro, L. Ruco, A. Villa, D. Simmons, and E. Deiana.** 1998. Junctional adhesion molecule, a novel member of the immunoglobulin superfamily that distributes at intercellular junctions and modulates monocyte transmigration. J. Cell Biol. **142:**117–127.
33. **Mitic, L. L., and J. M. Anderson.** 1998. Molecular structure of tight junctions. Annu. Rev. Physiol. **60:**121–142.
34. **Morita, K., M. Furuse, K. Fujimoto, and S. Tsukita.** 1999. Claudin multigene family encoding four-transmembrane domain protein components of tight junction strands. Proc. Natl. Acad. Sci. USA **96:**511–516.
35. **Nam, S. C., and K. W. Choi.** 2003. Interaction of Par-6 and Crumbs complexes is essential for photoreceptor morphogenesis in *Drosophila*. Development **130:**4363–4372.
36. **Nishimura, M., M. Kakizaki, Y. Ono, K. Morimoto, M. Takeuchi, Y. Inoue, T. Imai, and Y. Takai.** 2001. JEAP, a novel component of tight junctions in exocrine cells. J. Biol. Chem. **277:**5583–5587.
37. **Ohnishi, H., T. Nakahara, K. Furuse, H. Sasaki, S. Tsukita, and M. Furuse.** 2004. JACOP, a novel plaque protein localizing at the apical junctional complex with sequence similarity to cingulin. J. Biol. Chem. **279:**46014–46022.
38. **Perez-Moreno, M., C. Jamora, and E. Fuchs.** 2003. Orchestrating cellular signals at adherens junctions. Cell **112:**535–548.
39. **Ponting, C. P., C. Phillips, K. E. Davies, and D. J. Blake.** 1997. PDZ domains: targeting signalling molecules to sub-membranous sites. Bioessays **19:**469–479.
40. **Roh, M. H., C. Liu, S. Laurinec, and B. Margolis.** 2002. The carboxyl terminus of zonula occludens-3 binds and recruits a mammalian homologue of Discs Lost to tight junctions. J. Biol. Chem. **277:**17501–27509.
41. **Roh, M. H., O. Makarova, C. J. Liu, K. Shin, S. Lee, S. Laurinec, M. Goyal, R. Wiggins, and B. Margolis.** 2002. The MAGUK protein, Pals1, functions as an adapter, linking mammalian homologue of Crumbs and Discs Lost. J. Cell Biol. **157:**161–172.
42. **Saitou, M., Y. Ando-Akatsuka, M. Itoh, M. Furuse, J. Inazawa, K. Fujimoto, and S. Tsukita.** 1997. Mammalian occludin in epithelial cells: its expression and subcellular distribution. Eur. J. Cell Biol. **73:**222–231.
43. **Schneeberger, E. E., and R. D. Lynch.** 1992. Structure, function, and regulation of cellular tight junctions. Am. J. Physiol. **262:**L647–L661.
44. **Staehelin, L. A.** 1974. Structure and function of intercellular junctions. Int. Rev. Cytol. **39:**191–283.
45. **Stevenson, B. R., J. D. Siliciano, M. S. Mooseker, and D. A. Goodenough.** 1986. Identification of ZO-1: a high molecular weight polypeptide associated with the tight junction (zonula occludens) in a variety of epithelia. J. Cell Biol. **103:**755–766.
46. **Takeichi, M.** 1991. Cadherin cell adhesion receptors as morphogenetic regulator. Science **251:**1451–1455.
47. **Taniguchi, M., M. Sanbo, S. Watanabe, I. Naruse, M. Mishima, and T. Yagi.** 1998. Efficient production of Cre-mediated site-directed recombinants through the utilization of the puromycin resistance gene, pac: a transient gene-integration marker for ES cells. Nucleic Acids Res. **26:**679–680.
48. **Tepass, U.** 2002. Adherens junctions: new insight into assembly, modulation and function. Bioessays **24:**690–695.
49. **Tsukita, S., and M. Furuse.** 1999. Occludin and claudins in tight junction strands: leading or supporting players? Trends Cell Biol. **9:**268–273.
50. **Tsukita, S., M. Furuse, and M. Itoh.** 2001. Multifunctional strands in tight junctions. Nat. Rev. Mol. Cell. Biol. **2:**285–293.
51. **Umeda, K., J. Ikenouchi, K. Furuse, H. Sasaki, M. Nakayama, T. Matsui, S. Tsukita, M. Furuse, and S. Tsukita.** 2006. ZO-1 and ZO-2 independently can determine whether and where claudins are polymerized into tight junction strands in polarized epithelia. Cell **126:**741–754.
52. **Umeda, K., T. Matsui, M. Nakayama, K. Furuse, H. Sasaki, M. Furuse, and S. Tsukita.** 2004. Establishment and characterization of cultured epithelial cells lacking expression of ZO-1. J. Biol. Chem. **279:**44785–44794.
53. **Wittchen, E. S., J. Haskins, and B. R. Stevenson.** 1999. Protein interaction at the tight junction. J. Biol. Chem. **274:**35179–35185.
54. **Wittchen, E. S., J. Haskins, and B. R. Stevenson.** 2000. Exogenous expression of the amino-terminal half of the tight junction protein ZO-3 perturbs junctional complex assembly. J. Cell Biol. **151:**825–836.
55. **Wittchen, E. S., J. Haskins, and B. R. Stevenson.** 2003. NZO-3 expression causes global changes to actin cytoskeleton in madin-darby canine kidney cells: linking a tight junction protein to Rho GTPases. Mol. Biol. Cell **14:**1757–1768.